INSTITUTE OF PHYSICS PUBLISHING SEMICONDUCTOR SCIENCE AND TECHNOLOGY

Semicond. Sci. Technol. **21** (2006) 550–557 doi:10.1088/0268-1242/21/4/023

Theoretical investigation of Schottky-barrier diode noise performance in external resonant circuits

P Shiktorov[1], E Starikov[1], V Gružinskis[1], S Pérez[2], T González[2], L Reggiani[3], L Varani[4] and J C Vaissière[4]

[1] Semiconductor Physics Institute, A Goštauto 11, 01108 Vilnius, Lithuania
[2] Departamento de Física Aplicada, Universidad de Salamanca, Plaza de la Merced s/n, 37008 Salamanca, Spain
[3] INFM—National Nanotechnology Laboratory, CNISM—Consorzio Nazionale Interuniversitario per le Scienze fisiche della Materia, Dipartimento di Ingegneria dell' Innovazione, Università di Lecce, Via Arnesano s/n, 73100 Lecce, Italy
[4] CEM2—Centre d'Electronique et de Micro-optoélectronique de Montpellier (CNRS UMR 5507), Université Montpellier II, 34095 Montpellier Cedex 5, France

Received 14 December 2005, in final form 7 February 2006
Published 8 March 2006
Online at stacks.iop.org/SST/21/550

Abstract
We report Monte Carlo simulations of electronic noise in heavily doped nanometric GaAs Schottky-barrier diodes (SBDs) recently proposed as promising devices for THz applications. We consider a SBD operating in series with a parallel output resonant circuit when a high-frequency large-signal voltage is applied to the whole system. Significant modifications of the noise spectrum with respect to the diode subjected to a constant applied voltage are found to occur in the THz-region. To interpret such behaviour, we have developed a simple analytical approach based on the static I–V and C–V relations as well as on the series resistance of the SBD.

1. Introduction

One of the most promising directions to develop solid-state sources of THz radiation working at room temperature makes use of frequency multiplication in GaAs Schottky-barrier diodes (SBDs) and similar structures [1–10]. To extract the high-frequency signal, the SBD is usually loaded by an output resonant circuit, and the optimal conditions for signal extraction are achieved by a proper choice of the parameters of that circuit. In such a situation, the extracted regular signal generated by the pumped SBD and the intrinsic electronic noise of the SBD overlap in the whole frequency range of interest. As a consequence, the intrinsic noise deteriorates the extraction of the signal from the noise level. Therefore, a theoretical investigation of the modifications of the intrinsic noise spectrum of the SBD embedded into the output circuit is a mandatory issue.

Many numerical tools allowing us to design and simulate the performance of SBDs embedded into linear circuits have been developed (see, e.g., [11, 12] and references therein). In such tools the SBD is typically described either by the elements of its equivalent circuit [11] or in the framework of a drift–diffusion model [12]. The intrinsic noise of the diode is usually represented by a set of equivalent noise sources of Norton or Thevenin type [11, 12]. These sources describe correctly the intrinsic noise spectrum only in the low-frequency region. By contrast, the high-frequency region in the sub- and near-THz band needs a detailed analysis of the kinetic processes occurring in the depletion and neutral regions of the SBD (see, e.g., [13]).

To account for the various physical processes, such an analysis is usually performed by the Monte Carlo particle (MCP) technique [14–16]. To this purpose, either static conditions, when only a dc voltage is applied to the SBD [16, 17], or the so-called cyclostationary conditions, when the SBD is also pumped by a large-signal periodic ac voltage [18], are considered. In both conditions, the current noise is found to exhibit a similar spectrum. At low frequencies this consists of a plateau corresponding to full shot-noise. At increasing frequencies, this plateau is limited by a noise increase with

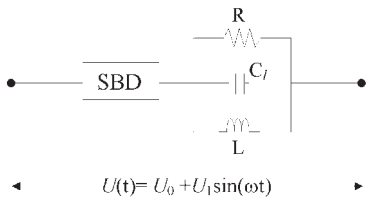

Figure 1. Scheme of the series connection of the SBD with a parallel resonant circuit.

a first maximum due to the resonance of carriers reflected by the Schottky barrier [13]. At the highest frequencies, before cut-off, there appears a second maximum due to a resonance originated by plasma oscillations belonging to the n^+n-homojunction [19]. However, in the case of circuit operation one can expect that, due to feedback, the output circuit should modify the SBD noise spectrum, especially under large-signal operation, where one can take advantage of frequency multiplication.

The aim of this paper is to investigate, in the whole frequency range of interest, the noise behaviour of the SBD embedded into an external output resonant circuit. For this sake, we use joint solutions of the equations describing the output circuit in the time domain, and MCP simulations of the instantaneous current flowing through the embedded SBD. In parallel, we also develop an analytical model of the SBD circuit operation that provides a physical interpretation of the numerical MCP results. For this task, starting from the simplest equivalent scheme of the SBD under test, we introduce the basic modifications necessary to obtain a qualitative and quantitative agreement with the numerical simulations of the whole system (MCP+circuit).

As a SBD we consider a nanometric GaAs n^+n-metal structure, the same as in [18], with n and n^+ region lengths of $l_n = 0.03$ μm and $l_{n^+} = 0.02$ μm, respectively, barrier height $U_b = 1.03$ V (built-in potential at the semiconductor–metal boundary), and carrier concentrations $n^+ = 8 \times 10^{18}$ cm^{-3} and $n = 1.1 \times 10^{18}$ cm^{-3}.

The paper is organized as follows. Section 2 presents the results of MCP simulations of the SBD noise in the output circuit. The analytical model is described in section 3, where it is discussed and validated by comparison with the results of the MCP simulation. Major conclusions are drawn in section 4.

2. Monte Carlo simulations

We consider a SBD in series with a parallel output resonant circuit consisting of a noiseless load resistance R, an inductance L and a capacitance C_l. This circuit is shown schematically in figure 1. A microwave voltage $U(t) = U_0 + U_1 \sin(2\pi\nu_0 t)$ of sufficiently high frequency ν_0 (typically in the 0.1–0.3 THz range; see, e.g., [1–10]) pumps the whole system (SBD+circuit). Due to its strongly nonlinear current–voltage (I–V) and capacitance–voltage (C–V) characteristics, the SBD generates a large number of high-order harmonics [18]. Here we shall consider mainly the case of frequency tripling when the output resonant circuit is tuned to the third harmonic of the fundamental signal at a frequency of $\nu_0 = 200$ GHz.

For this sake, in the framework of the MCP procedure for the SBD simulation, the Boltzmann transport equation self-consistently coupled with the Poisson equation is solved together with the output circuit equations in a similar way as reported in [20]. For the scheme presented in figure 1, the circuit equations can be written as

$$\begin{aligned} C_l \frac{\mathrm{d}U_c}{\mathrm{d}t} + j_L + \frac{U_c}{R} &= j_d \\ L \frac{\mathrm{d}j_L}{\mathrm{d}t} - U_c &= 0 \\ U_d + U_c &= U(t) \end{aligned} \tag{1}$$

where U_d and U_c are the voltage drops at the terminals of the SBD and the output circuit, respectively, j_L is the current density flowing through the inductance L, and

$$j_d(U_d, t) = j_d^{\mathrm{RS}}(t) + C_g \frac{\mathrm{d}U_d}{\mathrm{d}t} \tag{2}$$

is the total current density flowing through the SBD. Here $C_g = \epsilon\epsilon_0/(l_{n^+} + l_n)$ is the geometrical capacitance of the SBD and

$$j_d^{\mathrm{RS}}(t) = \frac{q}{(l_{n^+} + l_n)} \sum_{i=1}^{N(t)} v_i(t) \tag{3}$$

is the drift component of the current directly calculated by the MCP procedure in accordance with the Ramo–Shockley theorem [21, 22]. Here, $v_i(t)$ is the instantaneous velocity of the ith quasi-particle simulated by the MCP method, $N(t)$ is the number of quasi-particles inside the SBD at the time moment t, and q is the effective charge of the quasi-particle. The coupling of the circuit equations with the MCP procedure is carried out in a discrete time mesh $t_i = i\Delta t$. The sequence $j_d^{\mathrm{RS}}(t_i)$ is calculated by the MCP approach using the sequence of values of voltage drop at the SBD, $U_d(t_i)$, obtained by the solution of equation (1) on the time mesh. The convergence of such a scheme is controlled by decreasing the time step Δt. In accordance with [16], MCP simulations assume the contact of the n^+ region with the metal as Ohmic (cathode terminal of the SBD) and the boundary between the n region and the metal as perfectly absorbing (Schottky contact at the anode terminal). It is supposed that the whole voltage applied to the SBD drops between its terminals. This implies the presence of a surface charge at the metal–semiconductor boundaries (in the metal) which prevents the penetration of the electric field into the metal. As follows from equation (2), the time variation of this surface charge induced by the applied voltage is accounted for as a displacement current flowing through the geometrical capacitance C_g. In the framework of these boundary conditions, the calculation of $j_d^{\mathrm{RS}}(t)$ by the MCP procedure based on equation (3) accounts in a natural way for the following processes: first, the dynamical recharging of the SBD varactor capacitance related with the depletion region and the presence of the spreading (series) resistance caused by the neutral region of the diode; second, the fluctuations of the current caused by scattering of carriers.

In calculations, the capacitance of the output circuit is $C_l = 0.5C_g$ and the tuning of the resonator is driven by the output inductance which, for the resonance at the frequency

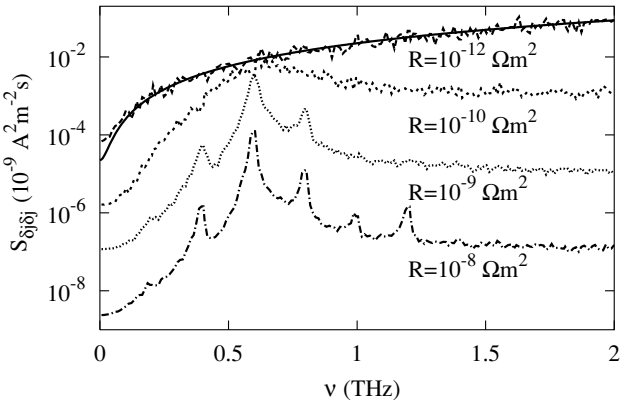

Figure 2. Spectral density of current fluctuations through load resistance $R = 10^{-12}$, 10^{-10}, 10^{-9} and 10^{-8} Ω m^2 calculated at $U_0 = 0.6$ V, $U_1 = 0.2$ V and $\nu_0 = 200$ GHz when the parallel circuit exhibits a resonance at the third harmonic.

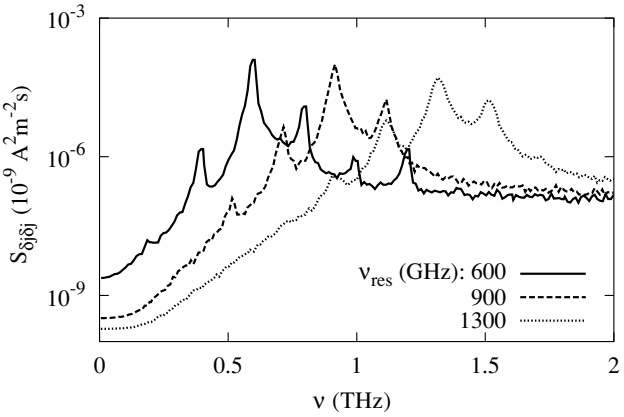

Figure 3. Spectral density of current fluctuations through the load resistance $R = 10^{-8}$ Ω m^2 calculated at $U_0 = 0.6$ V, $U_1 = 0.2$ V and $\nu_0 = 200$ GHz, and different $\nu_{\rm res} = 600$, 900 and 1300 GHz to which the parallel resonant circuit is tuned.

of the third harmonic, is given by $L = 1.02 \times 10^{-23}$ H m^2. (Here and below the SBD and circuit resistance, capacitance, and inductance are normalized to unit cross-sectional area; i.e., they are given, respectively, in units of Ω m^2, F m^{-2} and H m^2.)

By assuming that the output power generated by the SBD at the frequency of a given high-order harmonic is extracted from the load resistance R, the current (or voltage) fluctuations through (at the terminals of) this resistance are of most importance. Accordingly, figure 2 reports the results of MCP simulations for the spectral density of current fluctuations $S^R_{\delta j \delta j}(\nu)$ through the load resistance R when the resonant circuit is tuned to the third harmonic of the fundamental frequency. The curves refer, respectively, to the set of values: $R = 10^{-12}$, 10^{-10}, 10^{-9} and 10^{-8} Ω m^2. The spectra are calculated by making the finite Fourier transform (FT) [23] of the fluctuating current density $j_R(t)$ flowing through the resistance R. The spectral resolution is determined by the time interval $T = 500$ ps used to perform the FT. For simplicity, only the noise part of the spectrum is shown (i.e., the vertical spikes corresponding to regular contributions of the fundamental and high-order harmonics [23] are omitted). For comparison, the solid line reports the spectral density of current fluctuations for the SBD under the same pumping conditions $U_0 = 0.6$ V, $U_1 = 0.2$ V and $\nu_0 = 200$ GHz when the embedding circuit is absent and all the pumping voltage $U(t)$ drops only at the SBD terminals (below we shall refer to this situation as unloaded SBD).

When the load resistance is very small, the spectrum of $S^R_{\delta j \delta j}(\nu)$ practically coincides with the spectral density $S_{\delta j \delta j}(\nu)$ of the unloaded SBD (see, respectively, the curve for $R = 10^{-12}$ Ω m^2 and solid line in figure 2). With the increase of R, we observe a suppression of the low- and high-frequency wings of the spectrum centred on the frequency of the third harmonic ($\nu = 600$ GHz in this case), as shown by the curve for $R = 10^{-10}$ Ω m^2. With a further increase of R, an additional suppression of the spectrum wings (and, in part, of the spectrum centre) is observed (see curves for $R = 10^{-9}$ Ω m^2 and $R = 10^{-8}$ Ω m^2). Remarkably, at increasing values of R we observe the formation of a peak centred around the frequency of the third harmonic as well as the onset of a series of additional peaks centred around other harmonics. As follows from the comparison between the lower two curves, the greater the load resistance the higher the number of satellite peaks appearing in the spectrum.

Figure 3 reports the modification of the fluctuation spectrum $S^R_{\delta j \delta j}(\nu)$ due to the change of the resonant frequency $\nu_{\rm res}$ to which the output circuit is tuned. As follows from figure 3, the spectrum keeps the same structure when varying the resonant frequency even if this does not coincide with any frequency of the harmonics generated by the SBD (see curves corresponding to $\nu_{\rm res} = 900$ and 1300 GHz). With the increase of the resonant frequency, the peaks of the spectrum shift to higher frequencies following the main resonance $\nu_{\rm res}$ and keeping the same series at frequencies $\nu_{\rm res} \pm n\nu_0$ ($n = 1, 2, 3, \ldots$).

3. Analytical consideration

To provide a physical interpretation of the circuit noise spectrum obtained from MCP simulations, we start by considering a simple analytical model which assumes that the whole voltage applied to the SBD drops in the depletion region, thus neglecting the influence of the series resistance. Accordingly, the current flowing through the SBD can be approximated as:

$$j_d(U_d) = j^s_d(U_d) + \frac{\mathrm{d}}{\mathrm{d}t} Q^s(U_d) \tag{4}$$

where the drift component, $j^s_d(U_d)$, is taken from the static I–V relation, which neglects the current contribution caused by variations of the free carrier charge Q in the SBD. Since the model implies that the electric field in the neutral part of the SBD and in the cathode metal contact is equal to zero, the surface charge σ_s that prevents the electric field penetration into the metal is formed only at the Schottky-barrier contact and it is equal to the uncompensated charge Q^s of the depletion region, $\sigma_d = -Q^s(U_d)$. Therefore, the total SBD capacitance, defined in the framework of this model as $C_v(U_d) = \mathrm{d}Q^s(U_d)/\mathrm{d}U_d$, includes both the geometrical and varactor capacitances.

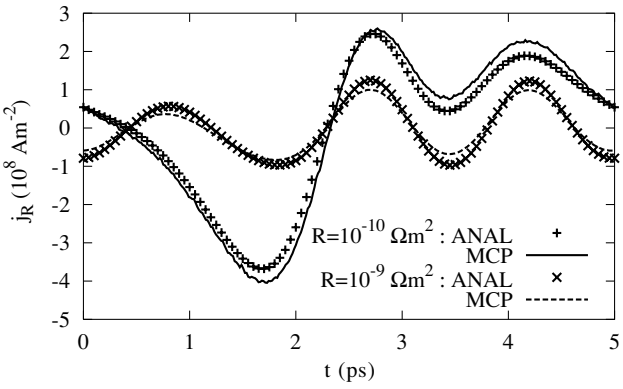

Figure 4. The regular part of the current flowing through the load resistance as a function of the time corresponding to one period of the applied voltage. Calculations are performed with $R = 10^{-10}$ and 10^{-9} Ω m^2 at $U_0 = 0.6$ V, $U_1 = 0.2$ V and $\nu_0 = 200$ GHz. Lines refer to MCP and symbols to analytically based approaches.

In case the SBD is loaded by the resonant circuit shown in figure 1, by using equations (1) and (4) $U_d(t)$ is found to satisfy the equation

$$\frac{\mathrm{d}^2}{\mathrm{d}t^2}[C_l U_d + Q^s] + \frac{1}{R}\frac{\mathrm{d}}{\mathrm{d}t}U_d + \frac{\mathrm{d}}{\mathrm{d}t}j_d^s + \frac{U_d}{L} = C_l\frac{\mathrm{d}^2}{\mathrm{d}t^2}U + \frac{1}{R}\frac{\mathrm{d}}{\mathrm{d}t}U + \frac{U}{L}. \tag{5}$$

To close equation (5), one needs to know the static relations $Q^s(U_d)$ and $j_d^s(U_d)$ and their derivatives with respect to U_d. For this sake, the static relations obtained from the MCP simulations under barrier-limited transport are approximated, respectively, by the standard analytical relations $j_d^s(U_d) \sim \exp(\beta U_d)$ and $C_v = bC_g/\sqrt{1 - U_d/U_{be}}$ with $\beta \approx 83V^{-1}$, $b \approx 1.5$, and $U_{be} = 0.97$ V obtained by optimizing the fitting.

Figure 4 compares the regular part of the current at the load resistance calculated directly from the MCP approach (lines) with that obtained by the analytical model based on equation (5) (symbols) for two values of the load resistance $R = 10^{-10}$ and 10^{-9} Ω m^2. The good agreement found validates the analytical model and justifies its use for the determination of the regular signal of the considered SBD embedded into the external circuit. Below we shall show that, with a proper intrinsic source of fluctuations, the analytical model allows us to evaluate also the circuit noise induced by the SBD.

To this purpose, let us suppose that the intrinsic noise source in the considered whole system is given by the fluctuations of the drift part of the current flowing through the SBD, δj_d. Since the pumping voltage does not fluctuate, i.e. $\delta U = 0$, after linearizing equation (5) for $\delta U_d(t)$ one obtains the following equation, which describes the fluctuations of the voltage drop between the SBD terminals,

$$\frac{\mathrm{d}^2}{\mathrm{d}t^2}[(C_l + C_v)\delta U_d] + \frac{\mathrm{d}}{\mathrm{d}t}\left[\left(\frac{1}{R} + \frac{1}{R_d}\right)\delta U_d\right] + \frac{1}{L}\delta U_d = -\frac{\mathrm{d}}{\mathrm{d}t}\delta j_d \tag{6}$$

where $R_d(U_d) = \left[\mathrm{d}j_d^s(U_d)/\mathrm{d}U_d\right]^{-1}$ is the differential resistance of the SBD depletion region. Due to the constraint $\delta U = 0$, the fluctuations of the voltage drop at the SBD and at the load resistance R are opposite in sign, i.e. $\delta U_R + \delta U_d = 0$. Thus, the fluctuations of the current flowing through R are described by $\delta j_R = -\delta U_d/R$. Since current fluctuations through the load resistance are governed by fluctuations of the voltage drop at the SBD, the spectrum of voltage fluctuations δU_d is the relevant quantity that describes the circuit noise.

The two main characteristics of the SBD, the capacitance $C_v(U_d)$ and the differential resistance $R_d(U_d)$, are time-periodic functions with the time dependence determined by the regular component of the voltage drop at the SBD, $U_d(t)$. Since, as shown in [18], in the frequency range of interest the main nonlinearity of the SBD considered here is determined primarily by the varactor capacitance, we can neglect the time dependence of $R_d[U_d(t)]$ assuming that R_d corresponds to the constant component determined by the static $j_d^s(U_d)$ relation averaged over the fundamental signal period $T_0 = 1/\nu_0$ as

$$\left(R_d^0\right)^{-1} = \frac{1}{T_0}\int_0^{T_0}\frac{\partial}{\partial U_d}j_d^s[U_d(t)]\,\mathrm{d}t = \beta\overline{j_d} \tag{7}$$

where $\overline{j}_d$ is the constant component of the current flowing through the SBD. (If necessary, the time dependence of R_d^{-1} in equation (6) can be accounted for in an analogous way as it will be done below for the varactor capacitance.) By following [11, 12], the time modulation of the SBD capacitance can be decomposed into a Fourier series as

$$C_v(t) = C_v^0\left[1 + \sum_{n\neq 0}^{\pm\infty}\gamma_n\exp(\mathrm{i}\omega_n t)\right] \tag{8}$$

where

$$C_v^0 = \frac{1}{T_0}\int_0^{T_0}\frac{\partial}{\partial U_d}Q^s[U_d(t)]\,\mathrm{d}t \tag{9}$$

is the constant component of the SBD capacitance and

$$\gamma_n = \frac{1}{T_0 C_v^0}\int_0^{T_0}\frac{\partial}{\partial U_d}Q^s[U_d(t)]\exp(-\mathrm{i}\omega_n t)\,\mathrm{d}t \tag{10}$$

is the relative contribution of the varying part of the SBD capacitance at the frequency of the nth harmonic of the pumping voltage, $\omega_n = n\omega_0$.

Within the above assumptions, equation (6) can be rewritten as

$$\frac{\mathrm{d}^2}{\mathrm{d}t^2}\left\{\left[1 + \frac{C_v^0}{\overline{C}}\sum_{n\neq 0}^{\pm\infty}\gamma_n\exp(\mathrm{i}\omega_n t)\right]\delta U_d(t)\right\} + \omega_{\mathrm{res}}^2\delta U_d(t) + \nu_{RC}\frac{\mathrm{d}}{\mathrm{d}t}\delta U_d(t) = -\frac{1}{\overline{C}}\frac{\mathrm{d}}{\mathrm{d}t}\delta j_d(t) \tag{11}$$

where $\overline{C} = C_l + C_v^0$, $\omega_{\mathrm{res}}^2 = 1/\overline{C}L$, $\overline{R} = RR_d^0/\left(R + R_d^0\right)$, $\nu_{RC} = 1/(\overline{C}\,\overline{R})$.

Equation (11) is equivalent to a nonhomogeneous linear differential equation of second order with time-dependent coefficients originated by an harmonic time modulation of the SBD varactor capacitance. By going to the frequency representation, such an equation can be reduced to the algebraic relations,

$$\delta U_d(\omega) = -Z(\omega)\left[\delta j_d(\omega) + \mathrm{i}\omega C_v^0\sum_{n\neq 0}^{\pm\infty}\gamma_n\delta U_d(\omega - \omega_n)\right] \tag{12}$$

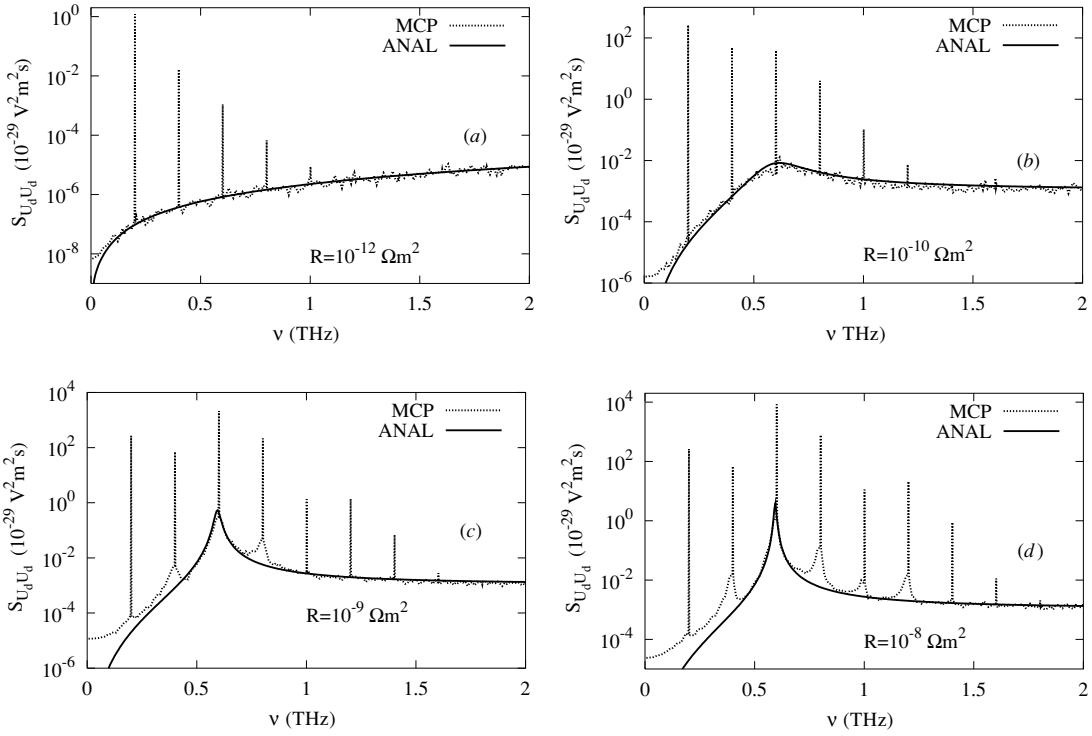

Figure 5. Spectral densities of the total voltage drop on the load resistor R calculated by the MCP technique (dotted curves) and by the analytical approach in the zero-order approximation (solid lines) for different values of R: (*a*) $R = 10^{-12}$, (*b*) 10^{-10}, (*c*) 10^{-9} and (*d*) 10^{-8} Ω m^2. $U_0 = 0.6$ V, $U_1 = 0.2$ V and $\nu_0 = 200$ GHz.

where

$$Z(\omega) = \frac{\mathrm{i}\omega}{\overline{C}\left(\omega_{\mathrm{res}}^2 - \omega^2 + \mathrm{i}\omega\nu_{RC}\right)} \tag{13}$$

is the net small-signal impedance of the whole system which describes the fluctuations of the voltage drop at the SBD. Let us consider the square brackets on the rhs of equation (12). Here, the first term corresponds to the intrinsic noise source. To characterize such a source we will use the spectral density of current fluctuations of the unloaded SBD, $S_{jj}^d(\omega)$, calculated by the MCP simulations under the same pumping conditions but in the absence of an output circuit. The second term describes the influence of the C–V nonlinearities on the voltage-drop fluctuations, $\delta U_d(\omega)$, due to the feedback originated by the output circuit for $R \neq 0$. As a consequence, the fluctuation $\delta U_d(\omega)$ at a given frequency ω is governed by the fluctuations of the same voltage drop at other frequencies shifted according to the harmonics generated by the varactor capacitance. Due to the frequency mixing involved in the second term of equation (12), the dependence of $\delta U_d(\omega)$ upon $\delta j_d(\omega)$ becomes implicit at a given frequency ω, but it remains linear with respect to the noise source.

Usually, such an implicit dependence can be resolved by using the conversion matrix method, which relates the sets of mixed frequencies (see, e.g., [11]). Here we shall use a less rigorous but more transparent approach based on sequential iterations with respect to the modulation coefficients γ_n of the varactor capacitance.

In the framework of the above approach, which allows us to obtain the whole output noise spectrum at each step, the jth and $(j-1)$th iterations of $\delta U_d^j(\omega)$ are related as

$$\delta U_d^j(\omega) = -Z(\omega)\left[\delta j_d(\omega) + \mathrm{i}\omega C_v^0 \sum_{n\neq 0}^{\pm\infty} \gamma_n \delta U_d^{j-1}(\omega - \omega_n)\right] \tag{14}$$

where, in the zero-order approximation corresponding to $\gamma_n = 0$, we use the following relation:

$$\delta U_d^0(\omega) = -Z(\omega)\delta j_d(\omega). \tag{15}$$

The spectral density of the voltage drop in the zero-order approximation takes the form

$$S_{U_dU_d}^0(\omega) = |Z(\omega)|^2 S_{jj}^d(\omega), \tag{16}$$

where $S_{jj}^d(\omega)$ is the spectral density of the intrinsic noise source. The spectrum $S_{U_dU_d}^0(\omega)$ corresponds to the usual linear transformation of the noise source spectrum by an embedded circuit in the absence of the frequency mixing caused by the C–V nonlinearity.

Figures 5(*a*)–(*d*) report the comparison between the $S_{U_dU_d}(\omega)$ obtained by MCP simulations and by analytical calculations in the zero-order approximation given by equation (16). Figure parts (*a*)–(*d*) refer to increasing values of the load resistance R. Here, the MCP spectra also include the contribution originated by the harmonics of the regular signal, as shown by the vertical spikes with spectral resolution $\delta\nu =$ 2 GHz. Calculations make use of the SBD parameters R_d^0 and C_v^0 obtained from the static I–V and C–V relations by means of equations (7) and (9) of the analytical model. The time dependence of the regular part of $U_d(t)$ used to

calculate R_d^0 and C_v^0 is obtained from the analytical model of the SBD circuit operation described by equation (5) and the analytical approximation of the I–V and C–V relations previously explained. For the SBD considered here, it is found that $C_v^0 \approx 6 \times 10^{-3} F/m^2$ and R_d^0 varies from 10^{-7} to 10^{-6} (Ωm^2) depending on the circuit operation conditions. Therefore, practically in the whole frequency range of interest $\omega C_v^0 R_d^0 > 1$, so that the impedance of the depletion region is mainly determined by the varactor capacitance $Z_d^0(\omega) = R_d^0/\left(1 + \mathrm{i}\omega R_d^0 C_v^0\right) \approx 1/\mathrm{i}\omega C_v^0$.

As follows from figure 5, the zero-order approximation provides a satisfactory description of the $S_{U_d U_d}(\omega)$ spectrum in practically the whole frequency range of interest, including the resonant frequency $\omega_{\mathrm{res}} = 3\omega_0$ at which the output circuit is tuned. The features of the $S_{U_d U_d}(\omega)$ spectrum are mainly determined by the frequency dependence of the net small-signal impedance $Z(\omega)$. However, with the increase of R, the zero-order approximation for $S_{U_d U_d}(\omega)$ is found to differ from MCP simulations in three main aspects:

(i) With the increase of the resonator quality ($R > 10^{-9}$ Ω m^2, see figures 5(c) and (d)) and the resonant frequency (see figure 8 below), the analytical model begins to overestimate the noise intensity at the resonant frequency ν_{res}.

(ii) Noise contributions with resonance shape, not predicted by the zero-order approximation, appear around frequencies $\nu_{\mathrm{res}} \pm n\nu_0$ (see figures 5(c) and (d)).

(iii) In the low-frequency region ($\nu \leqslant 0.5$ THz), the noise level predicted by the analytical model with the noise source $S_{jj}^d(\omega)$ unperturbed by the embedded circuit is lower than that obtained by MCP results. Note that in accordance with equations (13) and (16) when $\omega \to 0$ the spectral density $S_{U_d U_d}(\omega) \sim \omega^2$ and it must also tend to zero. The nonzero values of $S_{U_d U_d}(\omega)$ at low frequencies obtained in the MCP calculations reported in figures 2, 3 and 5 are caused by the limited accuracy of calculations that is inherent to the low-frequency region $\nu < 0.1$ THz.

To understand the origin of these discrepancies, let us first estimate the influence of the C–V nonlinearity on the noise spectrum by considering successive iterations in the framework of the same analytical model. Accordingly, the first-order approximation is obtained by substituting the expression for $\delta U_d^0(\omega)$ given by equation (15) into the rhs of equation (14). We obtain

$$\delta U_d^1(\omega) = -Z(\omega) \times \left[\delta j_d(\omega) - \mathrm{i}\omega C_v^0 \sum_{n\neq 0}^{\pm\infty} \gamma_n Z(\omega - \omega_n)\delta j_d(\omega - \omega_n)\right]. \quad (17)$$

By using the standard assumption that the noise sources $\delta j_d(\omega)$ corresponding to two different frequencies ω and $\omega - \omega_n$ are uncorrelated, from equation (17) one obtains the analogue of equation (16) for the spectral density of fluctuations of the voltage drop at the SBD,

$$S_{U_d U_d}^1(\omega) = |Z(\omega)|^2\left[S_{jj}^d(\omega) + S_{jj}^v(\omega)\right] \quad (18)$$

where the term related with mixing,

$$S_{jj}^v(\omega) = \left(\omega C_v^0\right)^2 \sum_{n\neq 0}^{\pm\infty} |\gamma_n|^2 |Z(\omega - \omega_n)|^2 S_{jj}^d(\omega - \omega_n), \quad (19)$$

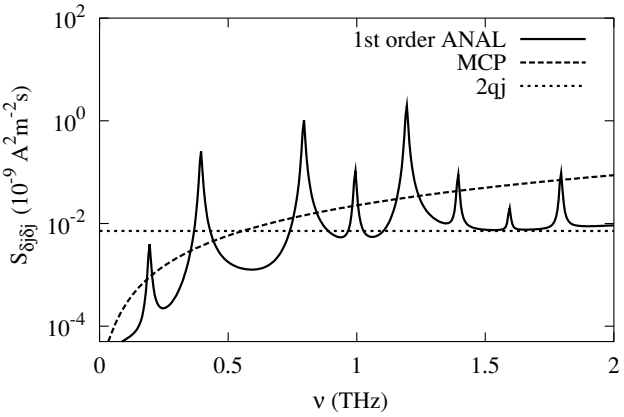

Figure 6. First-order iteration for the varactor component $S_{jj}^v(\omega)$ (solid line) in comparison with the unperturbed spectral density of current fluctuations $S_{jj}^d(\omega)$ (dashed line) and the shot-noise level under circuit operation (dotted line). $U_0 = 0.6$ V, $U_1 = 0.2$ V, $\nu_0 = 200$ GHz and $R = 10^{-8}$ Ω m^2.

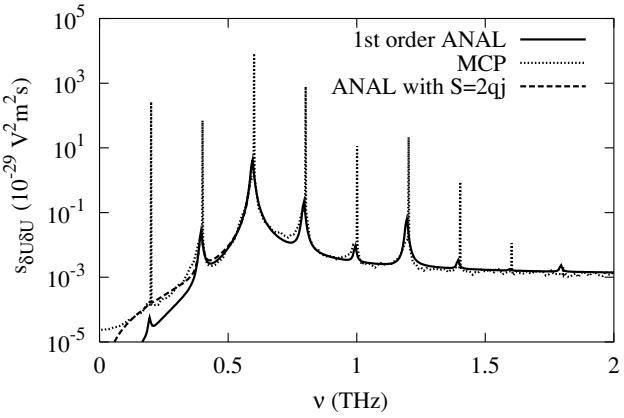

Figure 7. First-order iteration for $S_{U_d U_d}(\omega)$ (solid line) in comparison with the MCP results and first-order iteration with the improved shot-noise level (dotted and dashed lines, respectively). $R = 10^{-8}$ Ω m^2, $U_0 = 0.6$ V, $U_1 = 0.2$ V, $\nu_0 = 200$ GHz and $T = 500$ ps.

can be considered formally as an 'additional' source of fluctuations induced by the harmonic modulation of the varactor capacitance.

Figure 6 compares the intrinsic $\left(S_{jj}^d(\omega)\right)$ and the varactor $\left(S_{jj}^v(\omega)\right)$ components (dashed and solid lines, respectively) displayed on the rhs of equation (18). The γ_n-coefficients necessary to perform the calculations in accordance with equations (18) and (19) are obtained from equation (10) by using the SBD analytical model. As seen from figure 6, the spectrum of $S_{jj}^v(\omega)$ consists mainly of a set of resonance peaks which contribute to $S_{U_d U_d}(\omega)$ at frequencies $\omega = \omega_{\mathrm{res}} \pm n\omega_0$ ($n = 1, 2, \ldots$). Note that the contribution of $S_{jj}^v(\omega)$ at the frequency ν_{res} of the main resonance is negligibly small. Therefore, the first-order iteration modifies significantly the spectrum at the frequencies of the satellite spikes without changing in practice the main resonance. This is illustrated by figures 7 and 8, where $S_{U_d U_d}^1(\omega)$ obtained from the first-order iteration is compared with that of MCP simulations (respectively, solid and dotted lines).

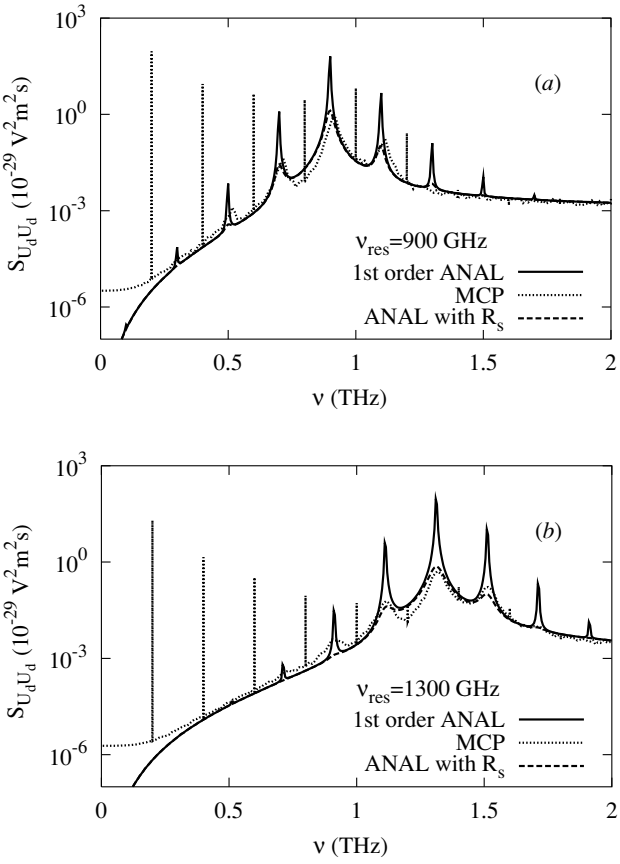

Figure 8. Spectral densities of the total voltage drop on the load resistor R calculated by the MCP technique (dotted curves) and by the analytical approach in the first-order approximation without and with the spreading resistance (solid and dashed lines, respectively) for two values of ν_{res}: (*a*) 900 and (*b*) 1300 GHz. $U_0 = 0.6$ V, $U_1 = 0.2$ V, $\nu_0 = 200$ GHz, $R = 10^{-8}$ Ω m^2 and $T = 2$ ns.

From the results reported in figures 7 and 8 we conclude that the first-order iteration gives merely a qualitative description of the origin of the resonant noise peaks at the frequencies $\omega = \omega_{res} \pm n\omega_0$. However, it overestimates their magnitude like in the zero-order approximation. Furthermore, this discrepancy sharply increases with the increase of the resonant frequency ν_{res} to which the output circuit is tuned (see figure 8). As proven by calculations, performing higher order iterations in equation (14) or making use of the conversion matrix method to solve equation (12) does not remove this discrepancy.

Accordingly, we will now show that the significant overestimate of the noise in all the resonant peaks is due to having neglected the spreading (series) resistance R_s of the SBD. To add R_s in series with the impedance of the depletion region, $Z_d^0(\omega) = R_d^0/\left(1 + i\omega R_d^0 C_v^0\right)$, in equation (12) of the above approach one must just replace the impedance $Z(\omega)$ with the expression

$$\tilde{Z}(\omega) = Z(\omega)\frac{1 + R_s/Z_d^0(\omega)}{1 + R_s Z(\omega)/\left[Z_d^0(\omega)Z_c(\omega)\right]} \qquad (20)$$

where $Z_c(\omega) = i\omega/\left(\omega_c^2 - \omega^2 + i\omega\nu_c\right)$ is the impedance of the output circuit in the absence of the SBD, $\omega_c^2 = 1/C_l L$, and $\nu_c = 1/C_l R$. In the zero-order approximation given by

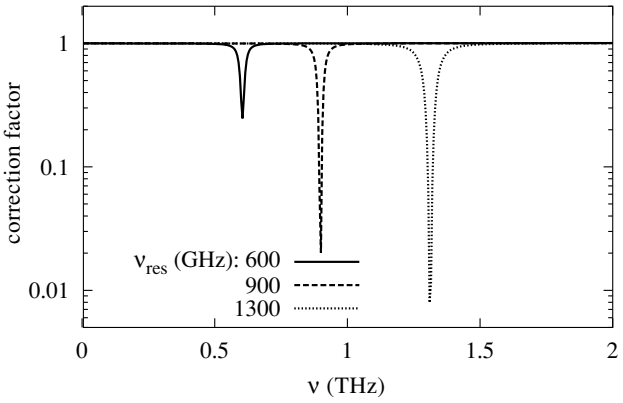

Figure 9. Frequency dependence of the correction factor caused by the spreading resistance $R_s = 10^{-12}$ Ω m^2 for the zero-order approximation at different values of ν_{res}. $U_0 = 0.6$ V, $U_1 = 0.2$ V, $\nu_0 = 200$ GHz and $R = 10^{-8}$ Ω m^2.

equation (16) the inclusion of the series resistance R_s leads to corrections in the fluctuation spectrum which can be described by the factor $\xi = |\tilde{Z}(\omega)/Z(\omega)|^2$. The frequency dependence of such a factor is reported in figure 9. Here, calculations are performed taking $R_s \sim 10^{-12}$ Ω m^2 as estimated by MCP simulations. As follows from figure 9, even for sufficiently small values of R_s we find a rather significant suppression of the peak at the main resonance frequency. Moreover, with the growth of the resonance frequency ν_{res} such a suppression increases. Outside the resonance region the influence of R_s is practically negligible. Calculations of $S_{U_dU_d}(\omega)$ performed in the first-order approximation given by equation (18) and accounting for R_s (see dashed lines in figure 8) are found to be in good quantitative agreement with MCP results (dotted lines) at both the main and satellite resonant frequencies. Since for the used value of R_s the cut-off frequency of the varactor capacitance $\omega_{cut} = 1/R_s C_v^0$ [24] is in the region of hundreds of THz, the observed suppression of the resonances is not related directly with the RC cut-off. This is also evidenced by the large intensity of the high-order harmonics presented in figures 7 and 8 by vertical lines.

We now consider the origin of the underestimate of the noise value at low frequencies, which is predicted by the analytical model with respect to the MCP results. This discrepancy is more pronounced when the output circuit is tuned to resonant frequencies $\nu_{res} \leqslant 600$ GHz (see figures 5 and 7). As shown in [18], under large-signal operation within the barrier-limited transport regime of the SBD, the noise value at low frequencies is governed by $\overline{j_d}$, in full agreement with the universal shot-noise law, $S_{jj}^d(0) = 2q\overline{j_d}$. By contrast, the noise spectrum at high frequencies, which includes the resonances originated by both carriers reflected from the barrier and plasma oscillations at the n^+n-homojunction, remains practically the same as that of the static case. Under resonant circuit operation, the voltage applied to the SBD depends on R, and thus it can differ significantly from the case of the unloaded SBD. Therefore, the underestimate of the low-frequency noise can be related with the increase of the mean current $\overline{j_d}$ associated with the increase of R, which is not accounted for by the noise source used above. To further illustrate this interpretation, figure 6 also presents

the shot-noise value $2q\overline{j_d}$ for the mean current value (dotted line) obtained from the SBD analytical model under circuit operation. As follows from figure 6, the current spectral density of the unloaded SBD underestimates significantly the real shot-noise value in the frequency region $\nu \leqslant 500$ GHz. By using the corrected shot-noise value one can recalculate the circuit noise in this region. The result is reported in figure 7 by the dash-dotted line, which practically coincides with the MCP results down to frequencies of about 0.1 THz.

4. Conclusions

In the framework of the Monte Carlo particle (MCP) technique coupled with the circuit equations, we have provided a theoretical investigation of the electronic noise generated by a SBD in the output circuit when the whole system (SBD+circuit) is pumped by a microwave voltage of frequency ω_0. By considering a heavily doped nanometric SBD, favourable to THz applications, we have found that under circuit operation the noise spectrum exhibits significant modifications with respect to the unloaded case. First of all, the output circuit leads to the appearance of a resonant behaviour of the noise spectrum at the frequency $\omega_{\rm res}$ to which the whole system is tuned. Moreover, with the increase of the resonator quality, an additional series of extra peaks centred at frequencies $\omega_{\rm res} \pm n\omega_0$ are found to appear. These are shifted with respect to the main resonance according to the frequencies of the fundamental and high-order harmonics of the pumping voltage.

We have developed a simple analytical model which is able to reproduce the main features of the noise spectrum generated in the output circuit by SBDs operating under barrier-limited conditions. The input parameters of the model, obtained from MCP simulations, are as follows: the static I–V and C–V relations, and the series resistance of the SBD. In particular, we have found the following: (i) the main resonance in the circuit noise spectrum is related to the usual linear transformation originated by the output circuit; (ii) the extra peaks appearing in the noise spectrum are caused by frequency mixing due to C–V nonlinearity, which induces a time modulation of the varactor capacitance of the SBD; (iii) even a very small value of the spreading resistance associated with the passive part of the SBD leads to a significant suppression of the noise in the main and satellite resonances, while having practically no influence on the remaining frequencies of the noise spectrum.

The analytical model is further improved by introducing as source of intrinsic noise of the SBD the spectral density of current fluctuations of the unloaded diode with the same pumping voltage as that applied under circuit operation. It is shown that such a noise source leads to a good estimation of the circuit noise in the intermediate and high-frequency region, where the SBD noise is determined by the resonant behaviour of free carriers in the neutral part of the SBD. In the low-frequency part of the spectrum, i.e. in the shot-noise plateau related to the depletion region, the dependence of the shot-noise value on the range of operation of the diode in the circuit becomes of importance and must be taken into account.

Acknowledgments

The authors wish to acknowledge the financial support of NATO Collaborative Linkage Grant PST.EAP.CLG 980629, grant no 41/249885 of the Programme SSHN 2005 of the French Ministère de la Jeunesse, de l'Education nationale et de la Recherche, the Italian Ministry of Education, University and Research (MIUR) under the project 'Noise models and measurements in nanostructures', the Dirección General de Investigación (MEC) and FEDER through project TEC2004-05231MIC and the Consejería de Cultura de la JCyL through project SA044A05.

References

[1] Crowe T W 1989 *Int. J. Infrared Millim. Waves* **10** 765
[2] Rydberg A, Lyons B N and Lidholm S U 1992 *IEEE Trans. Microw. Theory Tech.* **40** 827
[3] Jelenski A, Grub A, Krozer V and Hartnagel H L 1993 *IEEE Trans. Microw. Theory Tech.* **41** 549
[4] Gelmont B L, Woolard D L, Hesler J L and Crowe T W 1998 *IEEE Trans. Electron Devices* **45** 2521
[5] Crowe T W, Hesler J L, Weikle R W and Jones S H 1999 *Infrared Phys. Technol.* **40** 175
[6] Moussesian A, Wanke M C, Li Y, Chiao J-C, Allen S A, Crowe T W and Rutledge D B 1998 *IEEE Trans. Microw. Theory Tech.* **46** 1976
[7] Maiwald F, Lewen F, Vowinkel B, Jabs W, Paveljev D G, Winnewisser M and Winnewisser G 1999 *IEEE Microw. Guid. Wave Lett.* **9** 198–200
[8] Chattopadhyay G, Schlecht E, Gill J, Martin S, Maestrini A, Pikula D, Maiwald F and Mehdi I 2002 *IEEE Microw. Wirel. Compon. Lett.* **12** 117
[9] Chattopadhyay G, Schlecht E, Ward J S, Gill J J, Javadi H H S, Maiwald F and Mehdi I 2004 *IEEE Trans. Microw. Theory Tech.* **52** 1538
[10] Maestrini A, Ward J, Gill J, Javadi H, Schlecht E, Chattopadhyay G, Maiwald F, Erickson N R and Mehdi I 2004 *IEEE Microwave Wirel. Compon. Lett.* **14** 253
[11] Held D N and Kerr A B 1978 *IEEE Trans. Microw. Theory Tech.* **26** 49
[12] Graial J, Krozer V, Gonzalez E, Maldonado F and Gismero J 2000 *IEEE Trans. Microw. Theory Tech.* **48** 700
[13] Trippe M G, Bosman G and van der Ziel A 1986 *IEEE Trans. Microw. Theory Tech.* **34** 1183
[14] Fischetti M V and Laux S E 1988 *Phys. Rev.* B **38** 9721
[15] Jacoboni C and Lugli P 1989 *The Monte Carlo Method for Semiconductor Device Simulation (Springer Series in Computational Micro Electronics)* ed S Selberherr (Berlin: Springer)
[16] Gonzalez T and Pardo D 1996 *Solid-State Electron.* **39** 555
[17] Gonzalez T, Pardo D, Reggiani L and Varani L 1997 *J. Appl. Phys.* **82** 2349
[18] Shiktorov P, Starikov E, Gružinskis V, Pérez S, González T, Reggiani L, Varani L and Vaissière J C 2004 *IEEE Electron Device Lett.* **25** 1
[19] Starikov E, Shiktorov P, Gružinskis V, Nougier J P, Vaissiere J C, Varani L and Reggiani L 1995 *Appl. Phys. Lett.* **66** 2361
[20] Mitin V, Gružinskis V, Starikov E and Shiktorov P 1994 *J. Appl. Phys.* **75** 935
[21] Shockley W 1938 *J. Appl. Phys.* **9** 635
[22] Ramo S 1939 *Proc. IRE* **27** 584
[23] Shiktorov P, Starikov E, Gružinskis V, Pérez S, González T, Reggiani L, Varani L and Vaissière J C 2003 *IEEE Trans. Electron Devices* **50** 1171
[24] Champlin K S and Eisenstein G 1978 *IEEE Trans. Microw. Theory Tech.* **34** 1183